Electromechanical Energy Conversion Systems (EECS)
Niroo Research Institute (NRI)
Vol. 2, No. 1, Winter 2023, 9-28
DOI: 10.30503/eecs.2023.376522.1030
Review Article

Review of End Winding Forces Estimation in Synchronous Generators

Mehdi Aliahmadi[1], Alireza Ghaempanah[1*], Jawad Faiz[2]

Abstract

Increasing loading without comparable change in the size of synchronous generators, causes end-winding force estimation become important. Synchronous generators have been considered reliable if accurate end winding forces are evaluated and taken into account in the design process. The topic based on the current literature is reviewed. Structure of end windings and different analytical and numerical techniques for forces estimation are discussed. The current state of the art is reviewed and more successful developments are introduced. The area of research which needs more attention in the future to advance the subject is identified.

Keywords: Analytical methods, end winding, magnetic force estimation, synchronous generators.

Received Date: *13 December 2022;* ***Revised Date:*** *25 January 2023;* ***Accepted Date:*** *01 February 2023.*

1. INTRODUCTION

Enhancement of synchronous generators ratings without comparable geometrical increasing in the size of generators cause larger magnetic forces on end-coils. Therefore, design of an appropriate support to protect windings deterioration and damages by the above mentioned forces is critical. In slot-embedded portion of coils, the forces could be adjusted by teeth and slot wedges. Normally, the ends of coils have no external support and it is necessary to provide it. Two different types of induced forces on the coils are recognized. The first force caused by short circuit, especially at the generator terminals, have large amplitude and may destroy the coils. The second force is repetitive force caused by normal operation of the generator, which is relatively small but can damage the coils, especially its insulations. In addition, force caused by the normal operation could excite natural frequencies of windings structures and leads to serious damages. The force exerted on the stator coils is more important than those applied on the rotor; the reason is that the rotor end-coils are in a container called retaining rings which protect the rotor coils. The end-region structure of large synchronous generators is complicated, therefore some simplifications are required for computing its magnetic forces. These simplifications cause errors in the computed results. End region geometry of large synchronous generators can affect the magnetic force on end-coils. The literatures on the end-winding forces of large synchronous generators are reviewed. This review covers the modeling of end-windings, various criteria for estimating end-winding forces, and different analytical and numerical techniques for forces evaluation. Suggestions for the future works are proposed.

2. END-REGION STRUCTURE

In large synchronous generators the end-region generally consists of stator and rotor end windings, stator core end plates, rotor retaining rings, and stator frame. Two sides of the stator coils in end-region consist of a straight part emerged from the slot and followed by an involute curve laid upon the surface of a fictitious cone. At the end portion, two sides of the coil are joined together making a semi-diamond shape called nose (Fig. 1a). Each coil side comprises two bends, before starting and after terminating the involute portion, which are called first bend and second bend of the coil side. The rotor end windings contain retaining rings which are the most highly stressed component in the generator. Retaining rings hold the rotor end windings against centrifugal forces. The ring material in large generators is either magnetic or non-magnetic. The non-magnetic materials are

[1] Electrical Machines Research Department, Niroo Research Institute (NRI), Tehran, Iran
[2] Center of Excellence on Applied Electromagnetic Systems, School of Electrical and Computer Engineering, College of Engineering, University of Tehran, Tehran, Iran
*Corresponding author email: aghaempanah@nri.ac.ir

strong types which are used more than the magnetic materials [1]. Figure 1(b) exhibits the rotor end-windings. Fringing effects and end windings, in the end-region of the generators, particularly in the conical portion, produce axial magnetic flux which enters the stator core and induces eddy currents in the stator core teeth and stator yoke. Accordingly, additional undesirable losses in the stator core-end are generated and also lead to the magnetic saturation.

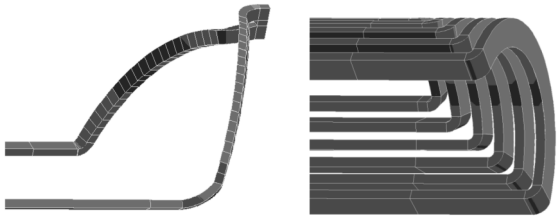

(a) (b)

Fig. 1. (a) Stator end winding coil, (b) Rotor end winding [2]

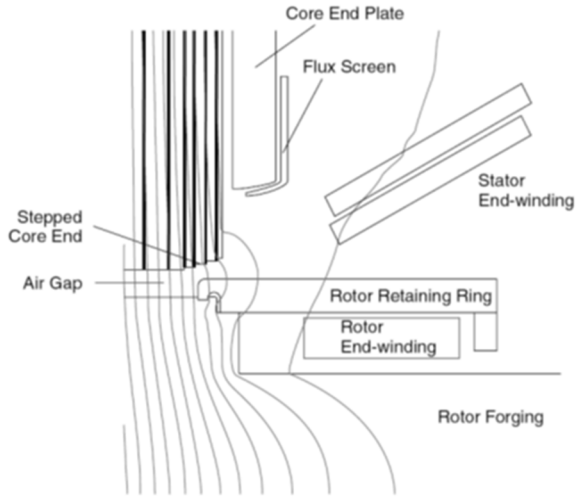

Fig. 2. Typical view of large synchronous generator end-region [1]

In order to avoid the above-mentioned effects, one can use an ideally infinite conductor screen or a highly permeable plate on the end plate; the former avoids entering the axial flux into the stator core owing to induced eddy currents in the conductor screen and the latter diverts the entering axial flux away from the stator core [1]. A typical view of a synchronous generator end-region has been illustrated in Fig. 2.

3. ESTIMATION OF FORCE EXERTED ON STATOR END-WINDINGS

In order to estimate the magnetic force exerted on the stator end-coils, three steps are followed. At the first step, the currents generating magnetic field in the end zone are determined. These currents comprise the stator and rotor currents as well as the eddy currents induced in the solid conducting parts of the end region such as rotor retaining ring and stator core end plate. It is apparent that these currents depend on the operating conditions of generator. The second step is computing the magnetic field in the end region and the third step is calculating the force exerted on the stator end windings.

The above-mentioned steps may be accomplished analytically or numerically as described in the following sub-sections.

3.1. Analytical Methods

Analytical methods were the first tools for describing the end-region magnetic field and estimating the exerted force. One of these methods uses Biot-Savart law to calculate the magnetic force. In this case, the magnetic flux density of a current-carrying conductor can be calculated as follow:

$$\vec{B} = \frac{\mu_0 I_1}{4\pi} \oint_{C_1} \frac{\overrightarrow{dl} \times \vec{R}}{R^3} \quad (1)$$

where

$\vec{B}$: Magnetic flux density

I_1 : Conductor current

$\overrightarrow{dl}$: Linear differential element of the conductor

$\vec{R}$: Distance vector from $\overrightarrow{dl}$ to the point in which the magnetic field is calculated

The differential magnetic force on a current-carrying conductor with current I_2 in the presence of the magnetic field can be calculated as follows:

$$\overrightarrow{dF} = I_2 \, \overrightarrow{dl} \times \vec{B} \quad (2)$$

where $\overrightarrow{dF}$ is the differential magnetic force. The magnetic force on conductor carrying current I_2 due to conductor carrying current I_1 can be calculated as:

$$\vec{F} = \frac{\mu_0 I_1 I_2}{4\pi} \oint_{C_1} \oint_{C_2} \frac{\overrightarrow{dl} \times \left(\overrightarrow{dl} \times \vec{R}_{12}\right)}{R_{12}^3} \quad (3)$$

where $\vec{R}_{12}$ is the vector from $\overrightarrow{dl}$ to $\overrightarrow{dl}$. According to (3), in 3-phase windings, the total magnetic force on an end-coil of a phase (e.g. phase A) depends on I_A^2, $I_A I_B$ and $I_A I_C$ so:

$$F_A = k_A I_A^2 + k_{AB} I_A I_B + k_{AC} I_A I_C \quad (4)$$

where

F_A: Magnetic force on a point of an end-coil in phase A
k_A, k_{AB}, k_{AC}: Coefficients depending on the conductor under consideration and position of the proposed point on that conductor
I_A, I_B, I_C: 3-phase currents

In the oldest analytical method [3], the conical portion of the end winding is approximated by infinite long straight conductors with the same distance between each two conductors; then by neglecting the effect of stator iron as well as considering the same current in each conductor (i.e. in line-to-neutral short-circuit and no-load conditions), the maximum tangential force exerted on each part is calculated by (3). These calculations are accomplished in a single layer of the end windings. It has been concluded that the estimated force on the first bend region, near the core, is the largest (Fig. 3) and toward the second bend of end coil (i.e. semi-diamond shape one) the direction of force is such that it tends to open the angle.
The simplified model of the conical portion of the end-winding [3] has been fairly improved in [4] by assuming that the stator end windings are laid on a surface-developed cylinder; the curved portion of each coil side is approximated by a 3-sectioned straight lines. Moreover, in order to calculate the maximum 2-D tangential magnetic force by (4), the effect of stator end-plate is taken into account by the images method [5,6] as an infinitely conducting area. However, the straight portion of coil, emerged from the slot, as well as the effect of retaining ring are neglected in the calculations. It has been asserted that the edge conductor in each phase belt experiences the largest force. Moreover, the effect of end-plate is almost on the first bend area of the end windings [4].

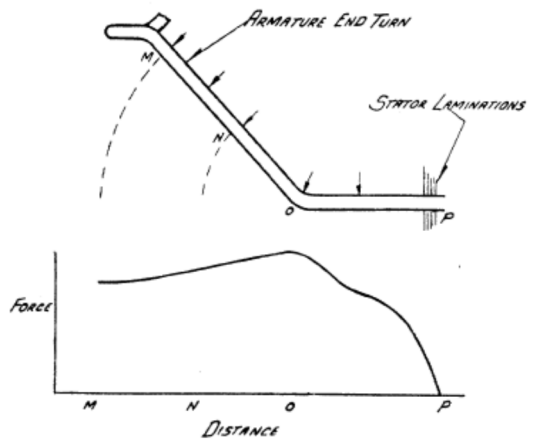

Fig. 3. Approximate magnetic force distribution on a coil side [3]

Magnetic field and force exerted on the conductors in the end region of a turbo generator using experimental results, was first studied in [7]. Based on the short circuit tests in no-load condition and different voltages, it was concluded that the circumferential magnetic forces, exerted on the first bend area of each end winding conductor, strain the groundwall insulation and decrease the insulation strength of the stator conductors in the end region.
The analytical method in [7] is on the basis of (4), in which, the magnetic force has been calculated in 3-D coordinates; nevertheless, the largest-existing force on the edge of a phase belt is as illustrated in [4]. In addition, the increment of radial force on the first bend area of the end windings due to the effect of magnetic rotor retaining ring was described using an experimental setup of stator and rotor end windings, which was supplied by an external short circuit generator.
One of the appropriate models for describing the stator and rotor end windings is representing the current carrying conductors as current sheets which was first introduced in a 2-D model by Young and Tompsett [7] and then in a 3-D model by Smith [8]. This method was subsequently used in [9,10] in order to simplify the complexity of conical portion of stator end windings by means of staircase current sheets. The magnetic field is computed by magnetic vector potential taking into consideration both the rotor and stator currents. However, the disadvantage of [10] is that it completely ignores the effect of iron, which has remarkable impacts on the distribution of the magnetic flux density in the end region and thereby on the magnetic force, while in [11] this method is used and boundary surface iron, specially magnetic ones, such as stator core end plate, rotor shaft, cylindrically surface of stator frame, and end bell are considered as an infinitely permeable and resistive material. It should be noted that, however, the rotor retaining ring was assumed to be non-magnetic. The studied method in [11], which is the extension of [12-14], is on the basis of calculating the 3-D magnetic flux density in the end region using the magnetic vector potential in cylindrical coordinates. At the first step, the stator and rotor end windings were replaced by equivalent current sheets using a simplified model of the end-region as shown in Fig. 4[12]. Stator end winding current sheets have been divided into three portions including axial and peripheral current sheets, radial current sheet and return current as illustrated in Fig. 5. The axial and peripheral current sheets are formed by ABCDE portion, radial current sheet is formed by EF

and GF portions and effect of the air gap is considered by a filamentary fictitious currents (i.e. FHG and FKG portions) called return current. The fundamental components of stator current sheets have been calculated using Figs. 5, 6 as follow [12]:

$$0 \le z \le b_s \quad \begin{cases} i_\theta = \theta & (5) \\ i_z = I_z \sin P \sin(\omega t - \theta) \quad \frac{A}{m} & (6) \end{cases}$$

$$b_s \le z \le a_s$$

$$\begin{cases} i_\theta = I_\theta \cos\left(P\left(1 - \frac{z - b_s}{c_s}\right)\right) \cos(\omega t - \theta) & (7) \\ i_z = I_z \sin\left(P\left(1 - \frac{z - b_s}{c_s}\right)\right) \sin(\omega t - \theta) & (8) \end{cases}$$

$$I_{\theta_g} = -I_\theta \frac{1}{P/c_s} \sin P \cos(\omega t - \theta) \quad A \qquad (9)$$

$$\rho_g \le \rho \le \rho_1 \qquad i_r = I_r \sin P\left(\frac{\rho_1}{\rho}\right) \sin(\omega t - \theta) \qquad (10)$$

where

i_θ : Stator peripheral current sheet component
I_θ : Stator peripheral current sheet coefficient
i_z : Stator axial current sheet component
I_z : Stator axial current sheet coefficient

I_{θ_g} : Stator return current
i_r : Stator radial current sheet component
I_r : Stator radial current sheet coefficient
$P = p\left(\frac{\pi}{2}\right)$
p : Fractional coil pitch

Fig. 4. Simplified model of the end-region [12]

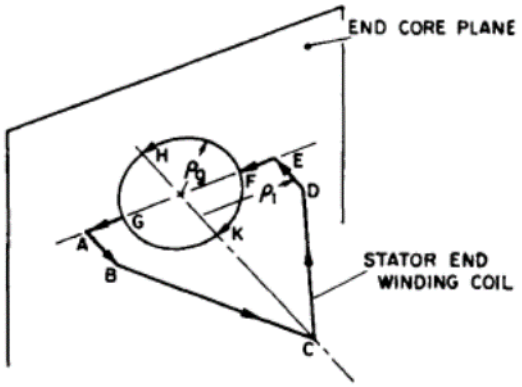

Fig. 5. Portions of the stator end winding coil [12]

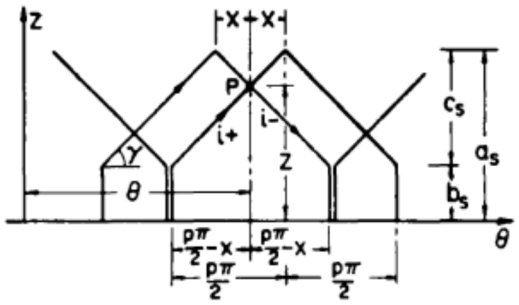

Fig. 6. Stator end winding configuration [12]

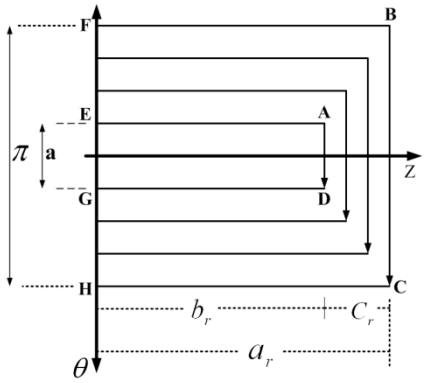

Fig. 7. Rotor end winding configuration

The fundamental components of rotor current sheets have been calculated using Fig.7 as follow [12]:

$$I_{\theta_{mg}} = -\frac{4}{\pi} \frac{I_{\theta_m}}{\frac{1}{2c_r}(\pi - a)} \cos\frac{a}{2} \cos(\omega t - \theta) \quad A \qquad (13)$$

$$i_{zm} = \frac{4}{\pi} I_{zm} \cos\frac{a}{2} \sin(\omega t - \theta) \quad \frac{A}{m} \quad 0 \le z \le b_r \qquad (14)$$

$$i_{zm} = \frac{4}{\pi} I_{zm} \cos\left[\frac{1}{2c_r}\left((\pi - a)(z - b_r) + c_r a\right)\right] \cos(\omega t - \theta) \qquad b_r \le z \le a_r \tag{15}$$

$$\rho_m \le \rho \le \rho_g \qquad i_{rm} = \frac{4}{\pi} I_{rm} \left(\frac{\rho_m}{\rho}\right) \cos\frac{a}{2} \sin(\omega t - \theta) \tag{16}$$

$\frac{A}{m}$

where

i_{θ_m}: Rotor peripheral current sheet component

I_{θ_m}: Rotor peripheral current sheet coefficient

$I_{\theta_{mg}}$: Rotor return current

i_{zm}: Rotor axial current sheet component

I_{zm}: Rotor axial current sheet coefficient

After calculating the stator and rotor end winding current sheets, the magnetic flux density in the end-region can be derived by calculating the magnetic vector potential in the end-region illustrated in Fig. 8 [11]. In this region, the magnetic vector potential is divided into two parts [11]. The first part is due to total current distributions confined between two infinite parallel planes as infinitely permeable boundary conditions. The second part of the magnetic vector potential is due to the total current distributions along with cylindrical boundary conditions. After calculating the magnetic flux density of each part of the magnetic vector potential, the total magnetic flux density is calculated as follow [11]:

$$\vec{B} = \vec{B}_1 + \vec{B}_2 \tag{17}$$

$$\vec{B}_r = \vec{B}_{1r} + \vec{B}_{2r} \tag{18}$$

$$\vec{B}_\varphi = \vec{B}_{1\varphi} + \vec{B}_{2\varphi} \tag{19}$$

$$\vec{B}_z = \vec{B}_{1z} + \vec{B}_{2z} \tag{20}$$

where

$\vec{B}_1$: Magnetic flux density of the first part of the magnetic vector potential

$\vec{B}_2$: Magnetic flux density of the second part of the magnetic vector potential

$\vec{B}_{1r}, \vec{B}_{1\varphi}, \vec{B}_{1z}$: Radial, peripheral and axial components of the magnetic flux density due to current distributions in the first part

$\vec{B}_{2r}, \vec{B}_{2\varphi}, \vec{B}_{2z}$: Radial, peripheral and axial components of the magnetic flux density due to current distributions in the second part

It was shown that the iron boundaries in the end region, except the stator core end plate, do not affect considerably the normal magnetic flux density in the stator end core. Moreover, because of replacing the stator end windings by a cylinder current sheet with a specific radius, calculated magnetic fields in the vicinity of actual conductors are not accurate. So it can be concluded that the method in [11] is not suitable for calculating the magnetic force on the stator end winding, because there are remarkable errors in the calculated magnetic field in the neighborhood of the conductors. Furthermore, incorrect calculated magnetic flux density close to air gap, due to replacing the air gap with circular filament, is another drawback of the method proposed in [11].

The above-mentioned drawback was resolved in [15] using more accurate model in which the stator end-windings were replaced by staircase current sheets as illustrated in Fig. 9. As a matter of fact, stator end windings are divided into several zones by surfaces of constant Z. Each zone comprises two cylindrical current sheet surfaces for each of outer and inner layer, including peripheral and axial current sheet, and connection between two zones of the same layer is accomplished by a radial current sheet. In addition, a radial current sheet is used in order to join the coil sides of an end coil.

It is noted that by using the above-mentioned method, magnetic field in some points can be determined on the center line of every end coil (i.e. one point in the middle of each zone). Thereby, the magnetic force exerted on each point can be calculated as follow:

$$\vec{F} = i\,\vec{l} \times \vec{B} \tag{21}$$

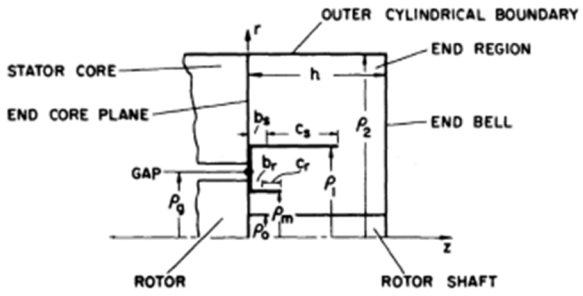

Fig. 8. End-region configuration [11]

where i is the current of the conductor in the center line, $\vec{B}$ is the magnetic flux density in the proposed point resulting from the all sources as well as induced currents in the end region, $\vec{l}$ is the axial distance of each zone, and $\vec{F}$ is the force exerted on each field point. [16] follows [15] by determination of exerted

magnetic force on the end conductors, following a 3-phase short circuit fault in no-load condition, based on (21). Thereby, the force components on a field point in cylindrical coordinates are [16]:

$$\vec{F}_r = -\frac{\left(\vec{B}_\varphi l_z - \vec{B}_z l_\varphi\right) I_L}{11.3} \times 10^6 \quad Pounds \tag{22}$$

$$\vec{F}_\varphi = -\frac{\left(\vec{B}_z l_r - \vec{B}_r l_z\right) I_L}{11.3} \times 10^6 \quad Pounds \tag{23}$$

$$\vec{F}_z = -\frac{\left(\vec{B}_r l_\varphi - \vec{B}_\varphi l_r\right) I_L}{11.3} \times 10^6 \quad Pounds \tag{24}$$

where

l_r, l_φ, l_z: Cylindrical components of the coil segment in which the field point lies

$\vec{B}_r, \vec{B}_\varphi, \vec{B}_z$: Cylindrical components of the magnetic flux density on the determined field point due to total current distribution in the end region

I_L: Current of the coil which the coil segment belongs to it

In [16], the magnetic force is determined for different ωt during the first cycle of the short circuit. In order to consider the transient rotor currents, it is assumed that these currents are induced in retaining ring so that the flux density remains unchanged at the starting time of the fault. It should be noted that in computing the short circuit current, subtransient condition has been neglected. The total resulting torque, using peripheral component of magnetic force during the first cycle of short circuit, which is arisen from stator and rotor currents, is shown in Fig. 10.

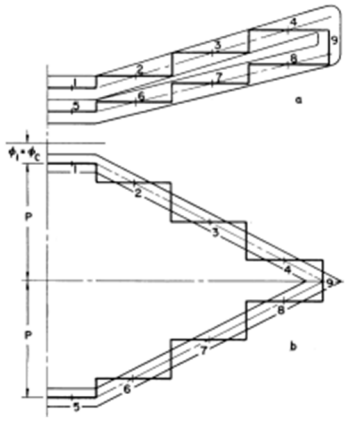

Fig. 9. Approximation of end windings with staircase current sheets [15]

The normal force which is important in design of braces is determined using the peripheral and axial forces [16].

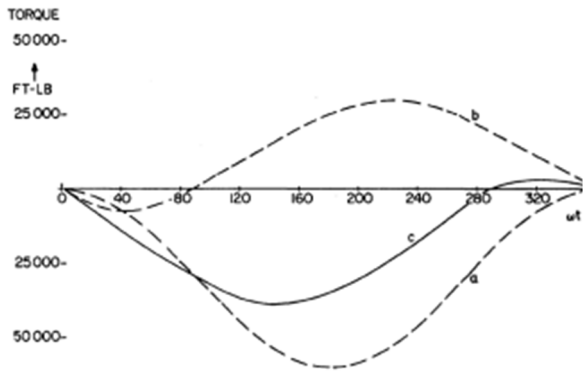

Fig. 10. Distribution of torque caused by: (a) stator currents, (b) rotor currents, and (c) total torque caused by stator and rotor currents [16]

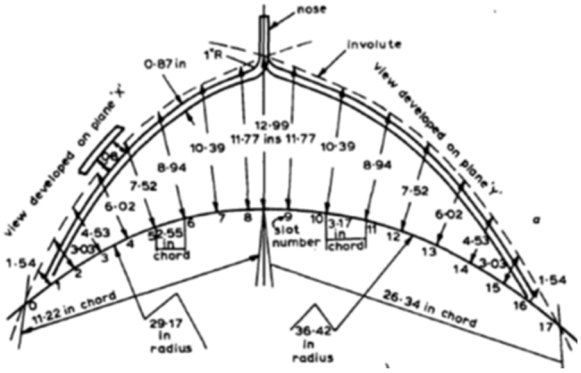

Fig. 11. Developed view of involute portion of the stator end winding [17]

In addition to the previously mentioned analytical methods for computation of the end region and force calculation, another method was studied in [17]. In this method, the magnetic field of the end windings is calculated by dividing the zero thickness filamentary conductors, instead of real conductors, into small straight segments (Fig. 11). The magnetic flux density in an arbitrary point due to a typical coil segment, as shown in Fig. 12, can be calculated as follow [17]:

$$\vec{B} = \frac{\mu_0 i}{4\pi} \int \frac{\vec{dl} \times \vec{R}}{\left|\vec{R}\right|^3} \tag{25}$$

$$\vec{B} = \frac{\mu_0 i}{4\pi} \cdot \frac{1}{FP} \left(\sin\theta_{n+1} - \sin\theta_n\right) \tag{26}$$

The actual shape of each conductor is almost made by combination of segments therefore this method can be applied to a conductor with any shape. The magnetic

field in each segment is calculated using Biot-Savart law and then the total field is computed by vector summation of the magnetic field of the segments. In this study, the harmonics of magnetic field have been also taken into account. Moreover, in order to include the iron effect, the image method was used. In fact, the effect of stator end plate and end of rotor body are considered as an infinite plane surface with an arbitrary permeability; whereas, the effect of nonmagnetic rotor retaining ring is neglected. The effect of the rotor shaft which is far from the stator windings is also neglected. The stator frame boundaries (i.e. both circumferential and end plates) are the boundary conditions which are ignored due to being in weak field area.

As is pointed out in [17], the fictitious current carrying conductor, considering the effect of air gap, is used when the end region surface has infinite permeability; because in the case of stator core end surface with infinitely conducting material, there are only radial and circumferential components of magnetic fields in the mentioned surface and the air gap has no effect on this magnetic field. Using the fictitious current carrying conductor for modeling the effect of air gap leads to a considerable error in computed fields in the vicinity of conductor (i.e. vicinity of the air gap). Since the rotor current is not considered in [17], the effect of power factor cannot also be investigated.

The method reported in [17] has been used to compute the magnetic force distribution in the end region [18]. In order to calculate the magnetic force, axial, radial and peripheral components of force density on the mid-point of each segment are estimated. The computed force densities on a segment due to other segments (the same coil or other coils) are added up to represent the total force on a segment. It can be concluded that in calculating the force, the first bend and distance between the first bend and starting point of involutes are not taken into account [18]. As a matter of fact, distribution of force density was calculated only in the conical and second bend portion of end winding.

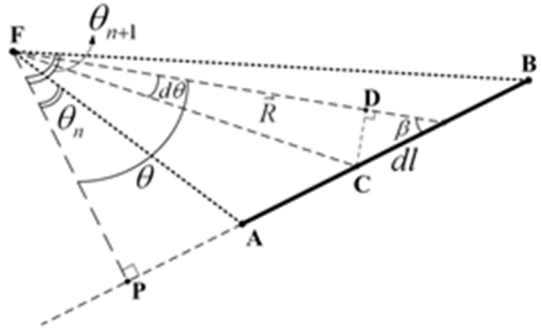

Fig. 12. An arbitrary field point F and a coil segment AB

As mentioned above, in order to decrease the computation time, the rectangular cross section of stator conductor end windings are replaced by their central filaments. It has been shown that the force between the filaments is always larger than the force between the rectangular conductors and there is 10% error in the estimated radial forces and 5% error in the calculated peripheral and axial forces.

Since the distribution of force density, considering $\mu = 1$ for stator end plate, lies midway between the force density considering the $\mu = 0$ and $\mu = \infty$, for simplification the force density has been calculated in [18] by ignoring the effect of the end plate iron. Regarding to the boundary condition, some simplifications are made. They are assumption of non-magnetic rotor retaining ring, and neglecting the effect of rotor shaft and stator frame [18]. These simplifications remove the complexity of the problem in the mentioned parts in the image method.

The stator end plate has the most impact on the axial force and least impact on the radial force. Furthermore, it has been asserted that the impact of retaining ring on the force density (except in the first bend region) is negligible compared to the rotor currents [18].

In the first step of force computation, as illustrated in Figures (13), (14), (15) and (16) [18], the magnetic force on the stator end coils, due to the stator currents, has been estimated and shown that the force distributions are different on each coil in the phase group as well as each side of a coil. The axial component of the force is the largest one and the acting force on the edge coils of a phase group is larger than that of the coils in the inner of a phase group.

Regarding to the influence of cone angle variation with force exerted, it has been illustrated that the radial force decreases with decreasing of the cone angle. However, relationship between the force and cone angle has not been given. In addition, the peripheral force component is hardly affected by the design parameters. Regarding to the effect of other winding design parameters including first straight portion, space between two layers and coil pitch, it was asserted that variation of straight portion is not significant, space between two layers is increasing due to the spacing reduction, and slight reduction of all components of the force due to reduction of coil pitch can be occur. It must be noted that, calculation of force due to the first straight portion was not involved in the [18].

To include the rotor currents in the estimated force on the stator end coil, 7 positions of the rotor related to the stator was considered in which the curved portion

of rotor end windings is approximated by the straight line. Magnitude of the force due to the rotor currents is small compared with that of stator current; in this case it was assumed that the eddy current effects in the rotor retaining ring are negligible. This assumption is not true in the subtransient conditions [18]. The effect of rotor current on the radial force is about 50% of that of the stator one. The axial and peripheral components are negligible. It has been asserted that the estimated force in subtransient condition (e.g. short circuit condition) is overestimated [18].

In evaluating the exerted magnetic force on the stator end-coils, it is worthwhile to compare two different methods (e.g. Biot-Savart law and 2D magnetic vector potential)[19]. In order to use Biot-Savart law, the current carrying conductors were divided into many short, straight elements. As shown in Fig. 17 and (27), the magnetic field in a current element j can be determined by the sum of the effect of all other current elements.

$$h_j = \frac{1}{4\pi}\sum_k i_k \frac{l_k \times r_{jk}}{|r_{jk}|^3} \tag{27}$$

where

h_j = Instantaneous magnetic field strength at element j

i_k = Current in element k

l_k = Length, in the current direction, of element k

r_{jk} = Radius vector between elements j and k $(k \neq j)$

The instantaneous force on current element j can be calculated as:

$$\boldsymbol{f_j} = \boldsymbol{i_j}.\boldsymbol{\mu_0}\left(\boldsymbol{I_j} \times \boldsymbol{h_j}\right) \tag{28}$$

In the above calculation, the effects of stator and rotor iron as well as the rotor current have been neglected.

In the magnetic vector potential method application, it has been assumed that the currents around the circumference of the end winding are constant. So the problem is reduced to 2-D problem, and only axial and radial components of force have been calculated. In this case, to include the effect of axial mmf traveling wave, some sinusoidally varying current rings are considered as illustrated in Fig. 18. The current rings and therefore the magnetic vector potential are both in the peripheral direction. The magnetic flux density is calculated using $\nabla \times \vec{A} = \vec{B}$ and then magnetic force density is determined. Comparisons of the application of two methods with experimental results were shown that the Biot-Savart method is closer to the experimental results than that of other methods. The analytical method proposed in [20] has been widely used, and the calculation results are well agreed with experimental results.

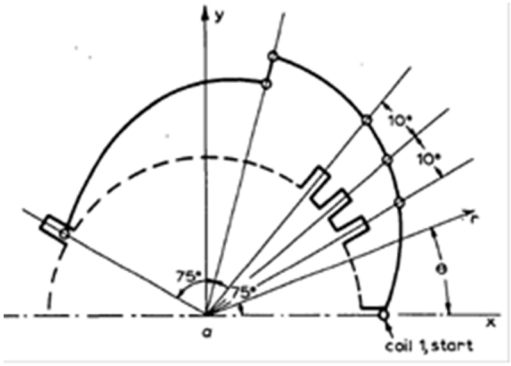

Fig. 13. Stator coil as a filament

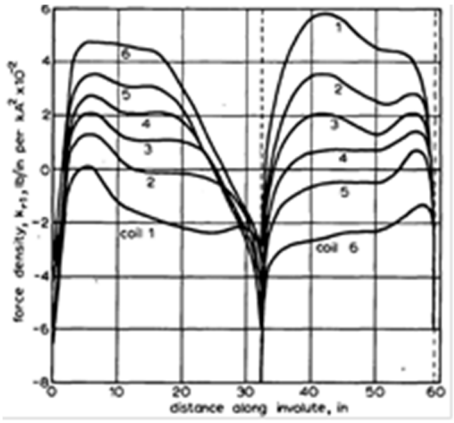

Fig. 14. Radial components of the force density of phase 1

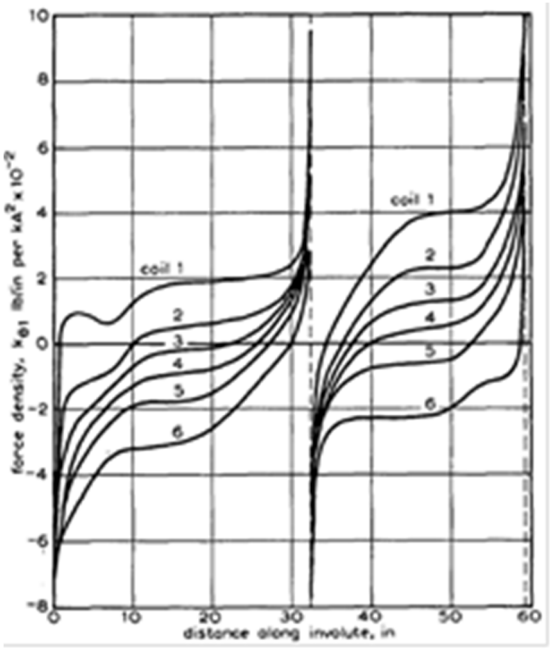

Fig. 15. peripheral components of the force density of phase 1

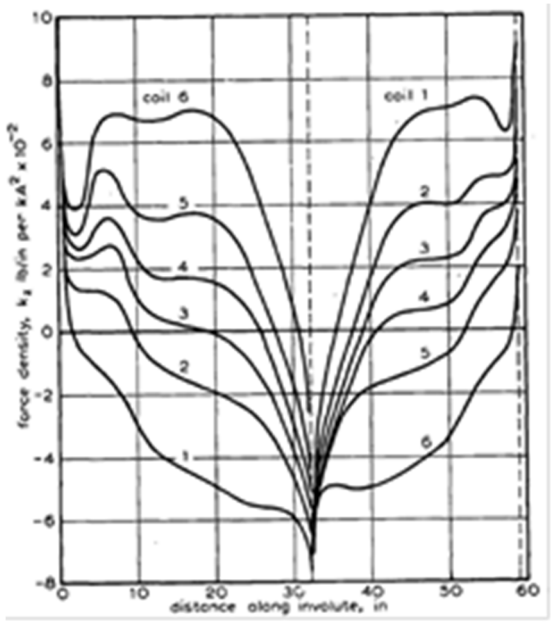

Fig. 16. Axial component of the force density of phase 1

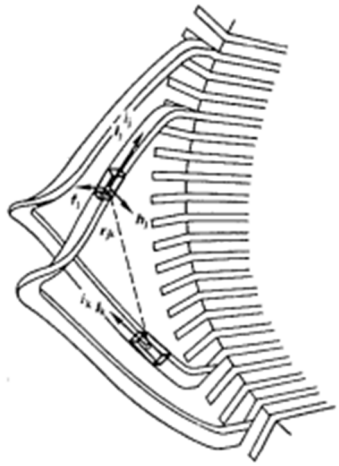

Fig. 17. Force on current-carrying element j due to element k [19]

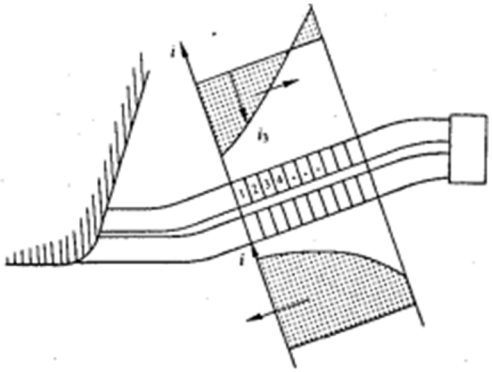

Fig. 18. Current ring for traveling mmf wave [19]

A quasi-static analysis of the magnetic field in the end region and acting magnetic force on the stator end windings can be accomplished for maximum stator current. In this case the empirical and analytical results were obtained. In order to acquire the experimental results, a 6-pole 800 kVA synchronous generator was used and the tests have been carried out at reduced voltage. It should be noted that, the practical results are acquired in 2-phase, 3-phase and in transition from 2-phase to 3-phase sudden short-circuit. The experimental results, in 3-phase short circuit, show that the tangential field between the poles is strong. This generates the strong radial forces on the stator end windings especially in the slot-exit straight portion. Although the maximum stator current in 2-phase short-circuit is lower than that of 3-phase fault, the distribution of the field components are almost similar to 3-phase fault thereof. Moreover, the axial field component is higher than that of the 3-phase short-circuit; also the total radial force is 10% higher than that of the 3-phase short-circuit case. In the case of transition from 2-phase to 3-phase short circuit, the field components are stronger than that of the 3-phase fault; it means that for axial component 24% and for radial and tangential components 60% stronger than that of the stress in 3-phase faults. The analytical calculation of the magnetic field in the end region is accomplished using Biot-Savart law [20]. The end-coil is approximated by the line conductor and the position vector of the involutes is used in Biot-Savart law. It was concluded that the measured value is 10-20% higher than that of the calculated value and it was asserted that the differences between the analytical and experimental results is due to the neglecting the effect of eddy currents in various portions of end windings. Therefore, the analytical method is only used for involutes portion of the end winding.

Analytical method, in conjunction with some experimental results, was used in [21] to estimate the magnetic force on the end-coils region of several hydro generators. This method is similar to that reported in [17] along with dividing the end-coil into four straight portions with rectangular cross sections as illustrated in Fig. 19.

Each section is divided into number of segments (filaments). The magnetic field in each filament in the presence of other filaments is calculated using the Bio-Savart law, where the effect of iron has been taken into consideration by image method. It is noted that the calculated values are higher than the measured values. These results are for 3-phase and phase-to-phase sudden short circuits. Distribution of the peak axial force density along the end winding in the coils of a phase belt during a sudden 3-phase fault is explained in [21]. Forces are computed in 3 first cycles and its

peak value is calculated in each rotor position angle. It was illustrated [21] that the maximum force for both layers of windings are at the end of phase belt near the first bend of the end coil. Furthermore, the distribution of the force density depends on the instant of fault occurrence. This effect is more significant in the phase-to-phase short circuit fault. This was followed by [22] to investigate the mechanical displacement and natural frequencies in the end windings. It was shown that in the short-circuit, the maximum stress would not excite the natural frequencies of the windings.

One of the magnetic field calculation method in the end region of a turbo generator in transient conditions was proposed in [23] in which the eddy current effect in the rotor retaining ring has been taken into account. This is done in the first cycle following the line-to-line or line-to-ground sudden short circuit faults. The first cycle of stator and rotor currents were considered and impact of rotor retaining ring eddy currents is investigated by considering a time delay in the resulting currents. Afterwards, the Fourier series of stator and rotor currents is obtained, and the magnetic field is calculated; then the magnetic force on the stator end winding is computed in [24] in three different stator short circuit conditions. It was shown that the maximum force is produced at half of the first cycle and on the edge of the phase belt conductors. Moreover, the exerted force in the case of line-to-ground fault has the largest and under 3-phase fault has the smallest value.

The above mentioned studies are used only analytical methods to describe the magnetic force in the end-region of a turbogenerator; however, it can be worthwhile to approve proposed method with a numerical one (e.g. finite element method) as proposed in [25]. It has been shown 10% difference between analytical and numerical methods. In addition, the effect of rotor retaining ring has also been investigated by using the model in two steps. At the first step the stator windings are omitted in the presence of rotor retaining ring and at the second step the rotor retaining ring is removed and the magnetic force is estimated in the presence of stator and rotor windings.

The other case which has not been dealt with is only calculating the magnetic field and magnetic force in the end region. These parameters, however, can be more valuable when were coupled with mechanical model of the end-region in order to investigate the vibrative behavior of stator end windings [26-28]. In this study the magnetic force has been calculated by Biot-Savart and Ampere's law; then estimated magnetic forces are used in mechanical modeling of the end-region.

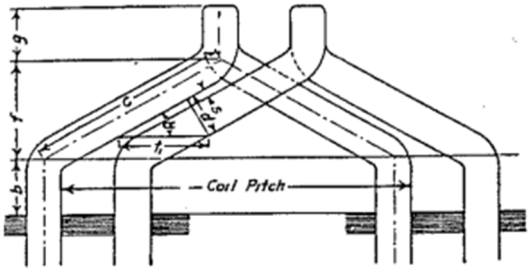

Fig. 19. End winding geometry[21]

3.2. Numerical methods

A quasi 3D numerical method has been developed to estimate the magnetic field of the end region and electromagnetic force exerted on the end coils of turbo generators [29]. Scalar magnetic field formulation has been used in [29] and it is assumed that the model is axisymmetric, leading to a two dimensional model. Furthermore, the magnetic scalar potential and all components of magnetic flux densities have been assumed sinusoidally distributed in the peripheral direction.

In the method, geometry of model is divided into rectangular cells and equivalent magnetic reluctance of the cell in any direction is replaced as shown in Fig. 20. Therefore, geometrical model is converted into an electric circuit where its nodes voltages are magnetic scalar potential of geometry nodes and elements currents are magnetic fluxes. Winding currents are considered as current sheets [12]. Since the magnetic scalar field formulation is valid only for the current-free regions, the value of scalar potential on the current sheets should be determined before solving the model. Values of these potentials are determined using a 2D permeance network with magnetic vector potential formulation. Fields of the stator and rotor currents are calculated in any point separately and sum of these two components in each direction with respect to a selected reference, gives the amplitude of the magnetic flux density components at that point. Calculated results have good correlation with the experimental results. The developed method can be used to predict the steady-state and transient magnetic field of the end region. Moreover, harmonic contents of the magnetic field can be taken into account. In the model two end-basket effects have been neglected. A quasi 3-D numerical method to estimate the steady-state electromagnetic force exerted on the stator end windings has been described in [30].

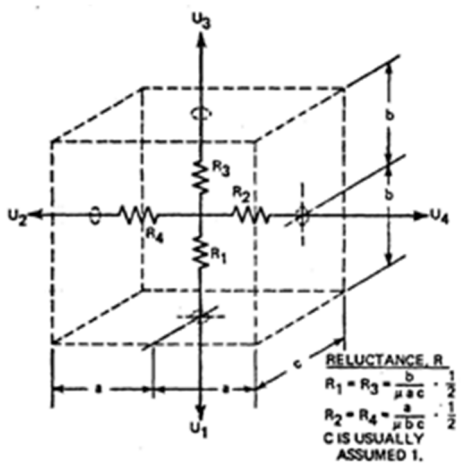

Fig. 20. 2-D reluctance model of the cell [29]

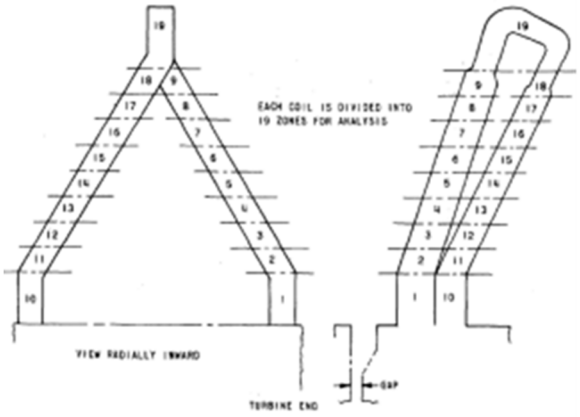

Fig. 21. Dividing end-coil into 19 zones [30]

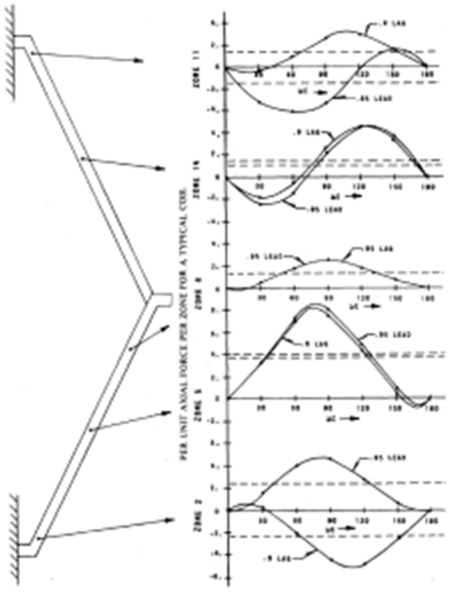

Fig. 22. Variation of force against power factor [30]

To simplify the problem, each coil is divided into 19 segments, 8 segments for conical portion of each side as shown in Fig. 21. However, the impact of the stator and rotor slots has been ignored. In order to calculate the magnetic field, finite difference technique for the scalar magnetic potential is used in accordance with axisymmetric and axiperiodic periodicity. It is assumed that the magnetic field in each direction is distributed sinusoidally in peripheral direction. In each segment of end coils, amplitude of magnetic field caused by both rotor and stator currents are computed separately. Sum of these two components according to a selected reference point for rotor angle, gives the net amplitude of the magnetic field in each zone.

The method is used to model the end-region of a 2 pole, 1000 MVA turbogenerator. Steady-state electromagnetic force is calculated using Ampere's law. The resulting force has two terms including an invariant and sinusoidally time-dependent terms. The latter term is oscillates sinusoidally with twice the frequency of the excitation frequency. In addition, effect of the power factor on the coil loading is studied as shown in Fig. 22. It can be seen that the phase difference at lagging and leading power factor near the core is larger than that of the other points of the end-coil. Also, the total peripheral and axial force on the coil at leading power factor is larger than the lagging power factor.

The extension of [30] has been proposed in [30] in order to analyze the transient condition of turbogenerator. Similar with the [30], end windings currents are replaced with a system of current sheets.

In a short circuit condition, stator currents has two direct and alternating components; thus, if current sheet method is used, modeling transient operation become complicated, because the alternating current sheet rotates with synchronous speed and direct component current sheet remains stationary. To overcome this problem, Park's transformations are applied to convert currents to qd0 currents, which are alternating but their positions are fixed in respect to the rotor position. It is assumed that the rotor current composes of two sinusoidal current sheets, one peaking in direct axis and another in quadrature axis. It is important to note that in the transient condition, forces and flux densities are not sinusoidally distributed and nor periodical, so anytime the computation should be done separately. Simulation results show that in a three phase short-circuit condition, electromagnetic forces exerted on the phase belts pull the belts together and net exerted force on

the phase coils tries to deform the coils as illustrated in Fig. 23.

Typical force pattern of different transient operation conditions in generators, are given for an 850 MVA, 24 kV, 2 pole generator in [31]. It has been found that expressing the results of simulations in force per slot pitch, is useful for compression of different transient conditions.

A quasi 3D FEM model for a 1000 MW and 2-pole turbogenerator has been developed in [32]. Geometry of the model includes the stator and rotor core and all peripherally solid components. Regions that have discontinuity in peripheral direction, such as rotor and stator tooth and slots are modeled with an equivalent permeability in peripheral direction that depends on the region geometries and material properties. Force is estimated in two steps; first, the magnetic flux densities in any point of the end region of generator are computed, and second the forces on the end-coils are evaluated using Ampere's law. Developed method can be used to estimate both steady-state and transient force induced on end-coils. It is assumed that the variables have sinusoidal distribution in the peripheral direction, thus as shown in Fig. 24, 3D end-region problem, reduces to 2D, where magnetic scalar potential formulations are used for simulation.

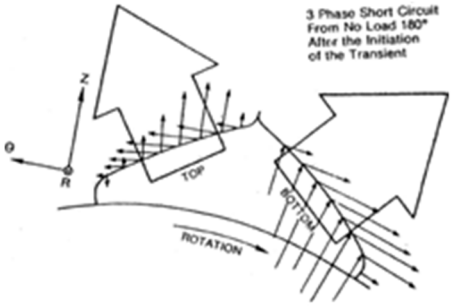

Fig. 23. Force tend to deform the coils [31]

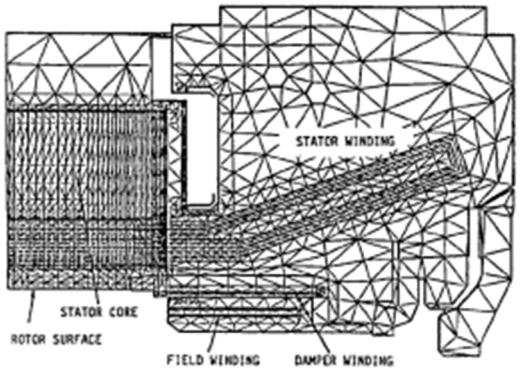

Fig. 24. End-region model of turbogenerator. [32]

Fault currents are computed using dq model of the generator with careful choice of the reactance and time constants. Suppose a three-phase short circuit fault occurs in a full-load generator when stator phase current is at negative going zero. All currents which are induced in the field windings, wedge, pole face dampers and rotor body are represented as lumped d and q damper windings. In modeling, each winding current is represented in the form of current sheets. In the case of top and bottom layer sides of stator coils, current sheets are positioned at radial center of each layer. Rotor field windings are split into two shells in radial direction located at 1/3rd and 2/3rd of radial depth of the windings. Modeling of damper currents is difficult if their exact geometries are considered. So, magnetic shell are derived using d and q equivalent damper mmf and positioned in line up with the rotor slot wedge. Any time winding mmf has sinusoidal distribution in the peripheral direction. Therefore, for accurate modeling, special attention must be paid to the proposed phase shift of the windings mmf, because of asymmetry in windings currents at fault conditions. Eddy currents in end region parts are included in the modeling; stator laminations are considered using an equivalent effective permeability which depends on the geometry and material properties of the stator laminations. For solid components, modified boundary condition related to the local permeability and their conductivity is defined. Also, it is assumed that the shaft surface is at zero scalar potential.

Results show that the axial component of the flux densities is largest component at straight portion of the stator. Peripheral component in annular space between the damper winding and bottom layer coils, near the end of active part of machine, has the largest component. Results of application of the method have good agreement with the measurements in both steady-state and transient conditions. Force on the end coils are calculated by dividing its geometry into a number of sections as shown in Fig. 25. Axial and radial force intensity components about half a pole pitch are shown in Fig. 26. Results show that the axial and peripheral components of the force burst the coils outward. Also, the peripheral component in phase belt tries to separate coils. In addition, the highest force is in the radial direction; however other components of the force are only slightly smaller and not in the same coil. For example at 0.01s highest force for radial, axial and peripheral components are 350 kN/m, 240 kN/m and 300 kN/m, respectively.

A 3-D mathematical model using integral-equation/singularity-method approach has been developed in [33]. Boundary condition that should satisfy is:

$$H \times N = 0 \tag{29}$$

where, H is the field intensity and N is the normal unit vector on the surface. To satisfy the above boundary condition, fictitious magnetic charge is distributed over the material-body surfaces. Magnetic field intensity is divided into two components as follow:

$$H = H_M + H_J \tag{30}$$

Where, H_J is the field intensity due to current carrying conductor and is calculated using Biot-Savart Law. H_M is the field intensity due to the fictitious magnetic charges and calculated as follow:

$$H_M = \nabla \int_S -\frac{M(Q)}{r_{PQ}} dS_Q \tag{31}$$

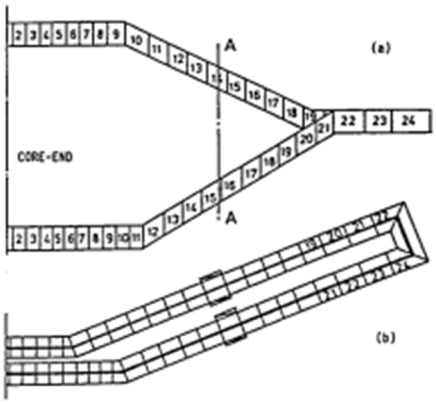

Fig. 25. Sections of stator coils for force calculation [32]

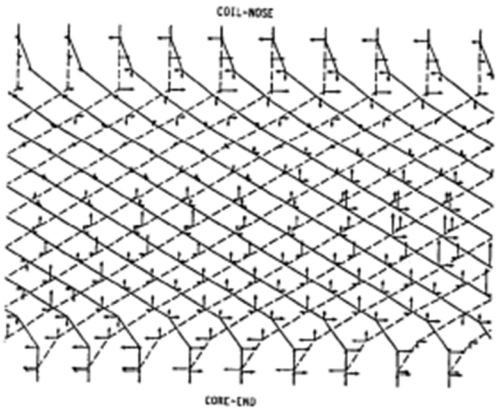

Fig. 26. Radial and axial force intensity about half a pole pitch at 0.01s [32]

M(Q) is the strength of the fictitious magnetic charge and r_{PQ} is the distance between point P and magnetic charge Q on the surface S. Selecting iteration formula for the integral equations and treatment of the singularity of the kernel of integral equations, are discrepancies of the developed method and other integral equation approaches. Singularities in the kernel are removed analytically, thus numerical iterations converge uniformly and need less storage capacity when complex geometries are modeled. In the developed method, permeability of the material bodies are assumed infinite and conductors are replaced by the infinitely thin current filaments.

In a case study the, magnetic field and force on the end-windings of a 850 MVA turbogenerator have been calculated. End-winding and end-region model has been shown in Fig. 27. In the developed method, the actual shape of end-coils is considered and the magnetic fields are calculated precisely. This is particularly important in regions between the top and bottom layers of basket, which is the main disadvantage of 2-D or quasi 3-D approaches that replaced winding currents with current sheets. Ampere's law is used to calculate the induced force on the end-coils. Results indicate that the force near the both ends of the conductor and phase centerline region is larger than other points. Fig. 28 shows the induced force on the top and bottom layer conductors at a constant distance from end of stator core.

A 3-D mathematical model using Integral equation method has been proposed in [34]. Eddy currents are ignored and the end-plate, rotor core and stator casing are considered by image method. The stator end-coils are divided into hexahedral bricks and modeled as solid parts, but the rotor field winding is represented by zero cross section filaments as shown in Fig. 29. Rotor damper windings are ignored. The rotor shaft is represented by 12 point prism elements.

The magnetic field intensity in the end-region is divided into two components, as follow:

$$H = H_C + H_M \tag{32}$$

H_C is the field intensity due to the stator and the rotor winding currents which is calculated by Biot-Savart law. H_M is the field intensity due to magnetization source and is calculated using integral equation. If the rotor is discretized as shown in Fig. 29, the integral equation reduced as:

$$H_c(P) + \sum_{i=1}^{n_M} G_{iP}\, M_i = \frac{1}{k_M} M_P \tag{33}$$

M is the magnetization vector and k_M is the magnetic susceptibility. By solving a system of equations based on (5), H_M can be obtained as follow:

$$H_M(P) = \sum_{i=1}^{n_M} G_{iP}\, M_i \qquad (34)$$

The force in any node of the stator winding is calculated by Lorentz law. Based on the FEM, the equivalent nodal forces are obtained as follows:

$$F_i^e = \int_{V_e} N_i b\, dV_e \qquad (35)$$

N_i is the shape function and b is the distributed Lorentz force. Nodal force results of implementation of the above method in the end-region of a 2 pole, 55 MW turbogenerator have been shown in Table 1.
Results have been calculated on the middle of phase A and B bars. A three-phase short-circuit occurs in a no-load generator at 0.01 s. short-circuit current is calculated using dq axis model. As shown in Table 1, ferromagnetic materials affect the results, especially for tangential and axial components of the force.
A 3D magnetostatic FEM with magnetic scalar formulation is used in [35] to estimate the force on the end-coils of 2pole, 600 MW turbogenerator at steady-state mode. The core saturation and induced eddy current in the coils and flux shield are ignored. The stator and rotor coils are replaced by filaments crossing the center of the coils as shown in Fig. 30. Impact of the rotor angle on the force is taken into account. Results show that the highest force densities are in the radial direction. In addition the force densities in other directions are slightly smaller than that of the radial component. The effect of core saturation, eddy current in the flux shield and stator slots on the magnetic field distribution at end-region and the force are studied.

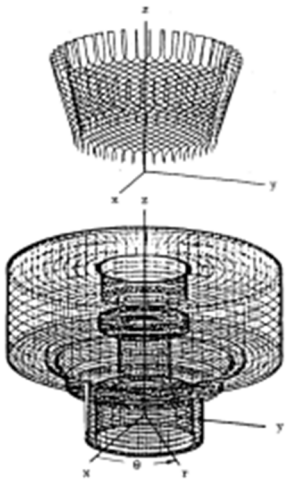

Fig. 27. End-winding and end-region boundaries [33]

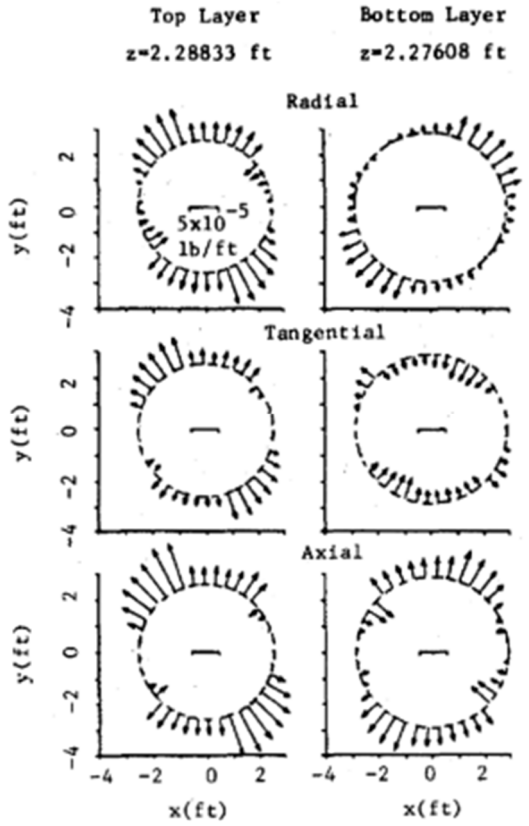

Fig. 28. Force distribution at a constant distance from end of the core [33]

Fig. 29. End-region, rotor and stator winding and rotor shaft [34]

It is stated that core saturation has induced 10% error near the core, in compression with linear magnetostatic model. Also flux shield induce 80% on the peripheral force and 20% on the radial force on the top layer coils on the basket. A 3D magnetic scalar formulation is used in [36] to predict the force exerted on a 600 MW turbogenerator under sudden no-load short-circuit condition. Short circuit currents of the windings are calculated using dq model or 2D FEM. therefore, as shown in Fig. 31, only considering the end of generator is enough for the flux density

distribution in the end-region. In the simulation, the eddy current in rotor teeth are neglected and stator and rotor teeth are assumed to be highly saturated, therefore a linear magnetic characteristics are considered. In addition, the rotor rotates at the synchronous speed.

Magnetic field at the end-region can be divided into two components; magnetic field generated by the windings currents and reaction field of iron and the induced eddy currents in the solid parts. The first component can be computed using Biot-Savart law, and the second component may be determined by the harmonic order frequencies of the induced eddy currents using Fourier series in a fix system, as follows:

$$j_f^s(r,\theta,z,t) = \sum_i j_f^s(r,z)\cos(\theta)\cos(\omega_i t + \varphi_i) = \\ = \sum_i \left(\frac{j_f^s(r,z)}{2}\cos(\omega_i t + \theta + \varphi_i) + \right. \\ \left. + \frac{j_f^s(r,z)}{2}\cos(\omega_i t - \theta + \varphi_i) \right) \quad (36)$$

$$j_f^r(r,\theta,z,t) = \sum_i j_f^r(r,z)\cos(\omega_r - \theta)\cos(\omega_i t + \varphi_i) \\ = \sum_i \left(\frac{j_f^r(r,z)}{2}\cos\big((\omega_i - \omega_r)t + \theta + \varphi_i\big) + \right. \\ \left. + \frac{j_f^r(r,z)}{2}\cos\big((\omega_i - \omega_r)t - \theta + \varphi_i\big) \right) \quad (37)$$

where i is the *ith* term of the series, j_f^s is the stator current density and j_f^r is the rotor current density. ω_r is the rotor angular speed. Based on (1) and (2), fundamental component of the eddy current induced in the solid parts are composed of four different rotating fields, two associated with the stator currents having frequencies ω_i which rotate forward and backward and two associated with rotor winding currents having frequencies (ω_i+ω_r) and (ω_i-ω_r), forward and backward rotating fields.

TABLE 1. NODAL FORCE AT TIME 0.01 S [34]

Phase-Slot-Layer	No ferrom. ele. [N]			With ferrom. ele. [N]		
	F_r	F_t	F_z	F_r	F_t	F_z
A-1-1	-584	-304	304	-586	-316	284
A-1-2	575	-370	-38	591	-330	-121
B-8-1	-275	-157	531	-300	-162	586
B-8-2	218	132	22	220	143	7

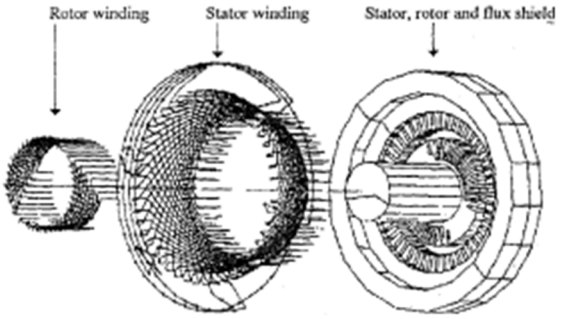

Fig. 30. Model of turbogenerator end-region [35]

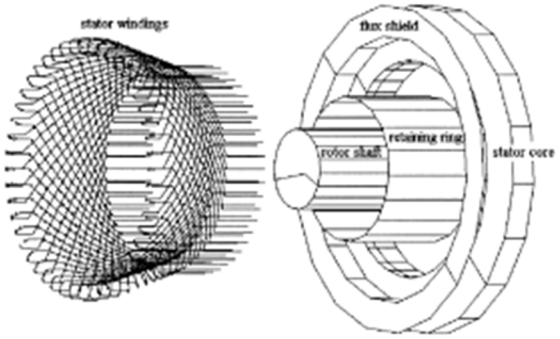

Fig. 31. Model of end-region of turbogenerator [36]

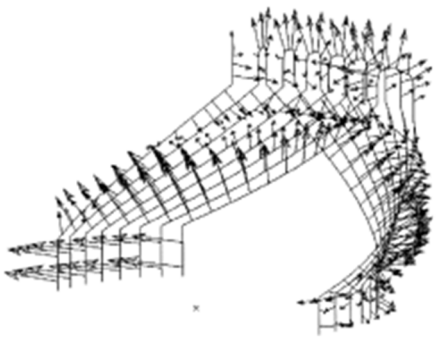

Fig. 32. Force on one stator pole at time 0.01s [36]

A modified Ohm law equation depending on the rotor and the rotating field speed is used as follows:

$$J = \sigma\left(1 + \varepsilon\frac{\omega}{\omega_r}\right) \quad (38)$$

where, $\varepsilon = +1$, if the excitation field and rotor rotate in the same direction and $\varepsilon = -1$ if they rotate in the opposite direction. By adding the response of the system to four rotating fields using modified Ohm law for input frequency ω_i and field generated by the windings currents, the magnetic flux density in any point of end-region is calculated.

Reduced scalar potential formulation is used to compute the magnetic field. In the modeling process, retaining ring and flux shield are modeled using a

magnetic shell and rotor shaft is modeled using the surface impedance method as shown in Fig. 29. Windings are represented by filaments; stator windings are excited by a three phase sinusoidal currents and rotor rotating fields are generated by two rotor windings having 90° apart from each other and carrying sinusoidal currents with 90° phase angle difference. For a correct representation of periodic signal, frequencies up to 100 Hz are considered; first frequency of Fourier series is 0.1 Hz and 14 other frequencies lower than 100 Hz is considered. Frequencies response was considered to be linear in sections. For each frequency magnetodynamic simulations are used. This model has 25,000 tetrahedral meshes. Results show that the force is maximized at 0.01 s following short-circuit fault. Fig. 32 shows the force distribution on one stator pole at this time. This force is fifty times larger than that of the steady-state condition. Maximum force density in three directions has the same order of magnitude. In the first cycle, high eddy currents are induced in the retaining ring. In addition force has three distinct components; include DC, 50 Hz and 100 Hz components.

A 3D magnetic scalar formulation are used to analyze the magnetic field distribution in the end-region of a 27 kVA, 4 pole synchronous generator in [37], in order to present the main characteristics of large synchronous generators. Some important features of small generator are: non-magnetic retaining ring, copper screen on stator core-end and its armature end windings are V-shaped.

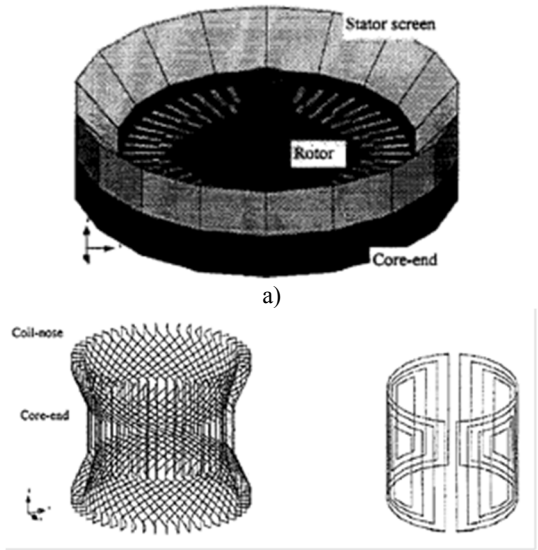

Fig. 33. a) end-region model, b) stator and rotor conductor representation [37]

It is assumed that the magnetic circuit is linear and retaining ring is perfectly permeable. In the modeling, only the end of machine is represented (Fig. 33). Stator screen and casing are supposed to be perfect screen for the magnetic field; therefore it is assumed that the normal component of the flux density on the surface of these regions is zero. Hence, only steady-state condition of the generator has been considered and damper windings are ignored. All generator conductors are modeled by replacing filaments crossing the center line as shown in Fig. 33.

In simulations, flux density distribution generated by each rotor winding and stator winding are studied and peak flux density is obtained. Also effect of removing copper screen, on the flux density distribution in the end-region is studied. Static formulation of FEM has been applied for simulation; therefore the eddy currents in solid parts are not modeled.

A 3D time harmonic FEM with reduced magnetic scalar potential formulation is used in [38], to calculate the end-winding force at normal operation of synchronous generator. Saturation of stator core and induced eddy current in solid parts of the end-region are considered. T, Φ-Φ formulation is used, considering the following assumption:

$$J = \nabla \times T_0 \tag{39}$$

where, J is current density. Static field intensity of each phase of stator winding is computed in any point using Biot-Savart law. If H_{S1}, H_{S2} and H_{S3} are the three phase stator winding magnetic field intensities at a point, equivalent time harmonic magnetic field intensity of the point is:

$$H_S = H_{S1} + H_{S2}e^{j120} + H_{S3}e^{j240} \tag{40}$$

The rotor winding excitation is considered as an equivalent T_0 vector which imposed on a thin layer on the surface of the rotor as shown in Fig. 34. It is sufficient to impose only first harmonic of radial component of T_0 vector on the thin layer as follows:

$$T_0 = t_0 e^{-jp\varphi} e_r \tag{41}$$

where, p is the rotor pole pair and e_r is the unit vector in the radial direction. To simulate arbitrary load condition, the magnetic field of rotor windings should be shifted by changing φ in (13), regarding to magnetic field of the stator winding.

Force exerted on the stator windings are calculated using Lorentz law. Calculated force contains two constant and oscillating components, latter component oscillate with twice the frequency of the excitation frequency. This part of the force is symmetrically

distributed over the stator slots as shown in Fig. 35a. Force densities near the rotor are peak (Fig. 35b).

A 3D vector potential finite element formulation is used in [39] to calculate the force on the end-winding of a 2 pole, 635 MVA turbogenerator. Simulations results have been presented for both steady-state and three-phase short-circuit conditions. Stator windings are modeled with the geometry of the real stator end-coils; shapes of the involutes part of coils are approximated the real shape, as shown in Fig. 36a. In order to shorten the simulation time, harmonic formulations instead of time-stepping technique have been used. Therefore, rotor field windings are replaced by the equivalent two phase ac windings as shown in Fig. 36b, separated 90^{O} from each other. It is assumed that the currents have on uniform distribution on the windings cross sections. Magnetic field in each region of model is computed for stator and rotor currents separately and results are added up based on the superposition principal. Ampere's law is used to calculate the force on the end-coil regions.

The results show that the radial force pattern on the end-coils is similar in both steady-state and three phase short circuit conditions as shown in Fig. 37.

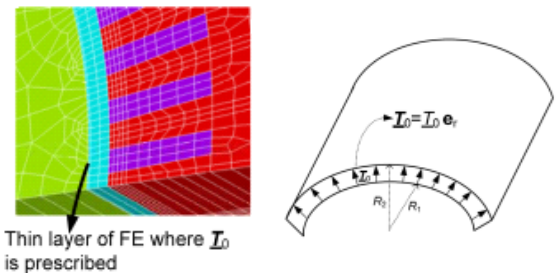

(a) (b)

Fig. 34. a) Thin layer of FE in the air-gap, b) Schematic presentation of prescribed T0. [38]

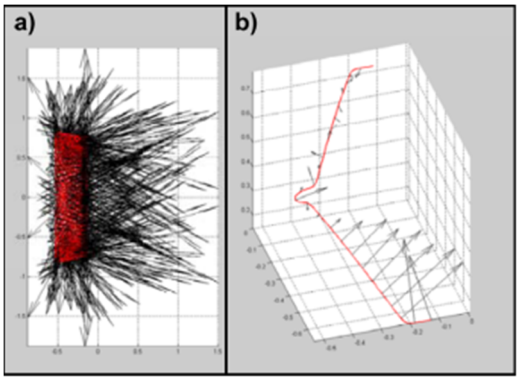

Fig. 35. a) Distribution of the force on the stator end-winding, b) force density distribution on a single winding. [38]

In the steady-state, the forces are such that some group coils attract each other, while other repel each other. In short circuit condition, the forces expand the coils of stator windings. Force on the adjacent coils is maximized when the two coils belong to different phases. In addition, torque in whole coil end is 22 times higher than that of the rated condition which is 15% of the machine rated torque. Dominate portion of the torque component is generated by the rotor currents.

A 3D magnetic vector potential formulation is used in [40] to study the force on the stator end-windings of a 200 MW turbogenerator in the steady-state condition, in lagging and leading power factors. The electromagnetic field is assumed to be in quasi-stationary and 3D steady-state FEM is used. It is assumed that all modeled materials have linear magnetic properties. Windings are modeled with real cross section, and involutes portion of end-winding are assumed to be straight as shown in Fig. 38. Last four stator packages are included in 3D model. Results contain forces exerted on the stator teeth, stator winding bending and top of the windings.

However, it is not clear that how the forces have been estimated in different parts. Also the effect of retaining ring, end shield, rotor shaft and casing are not taken into account in the calculation process. The results are0 not agreed with the experimental results or other methods.

Electromagnetic forces on the involute part of the end-winding of a 1550MW nuclear turbogenerator were investigated by using time-stepping finite element analysis in [41]. The obtained results show the importance of the upper and lower involute part of, respectively, the last coil and the first coil on which the exerted magnetic force is more crucial compared with other parts of the coils.

4. Discussion and Conclusion

Two and three dimensional magnetic field in the end region of a turbo generator and the resultant exerted magnetic force on the stator end-windings using analytical methods have been accomplished in the last years and decades. However, due to 3-D complicated structure of the end-region, 2D modeling of this region is not worthwhile. So, contributions in which 2-D models were used are not significant. When 3-D modeling of the end-region was used, modeling the end-winding from geometrical point of view, is important in determination of the exerted magnetic force on the end-windings.

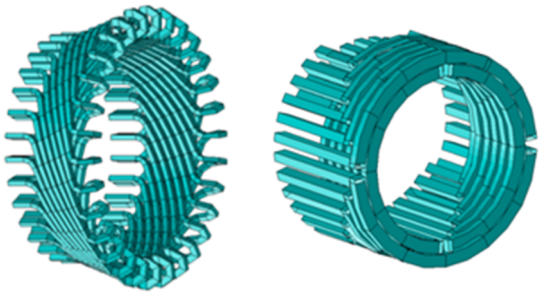

Fig. 36. Model of end-windings of turbogenerator, a) stator windings b) equivalent rotor windings [39]

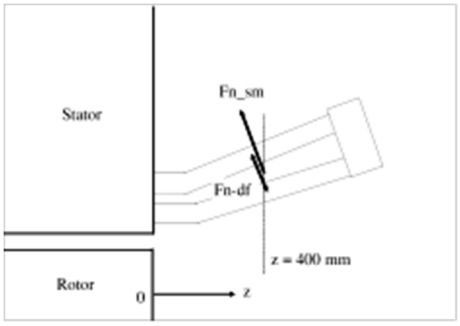

(a)

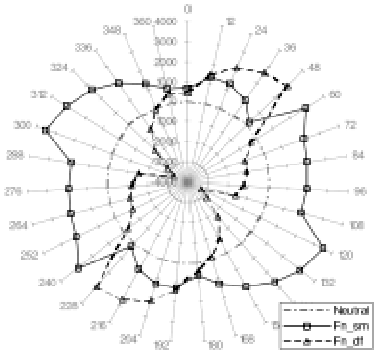

(b)

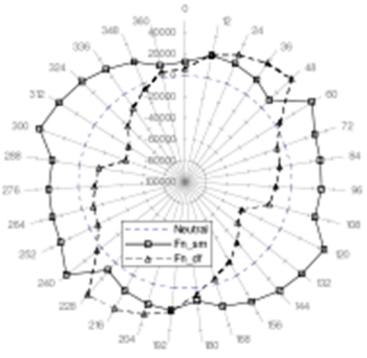

(c)

Fig. 37. Radial force pattern compression at steady-state and short-circuit, a) Points at which radial force are calculated, b) Radial force distribution at steady-state, c) Radial force distribution at short-circuit [39]

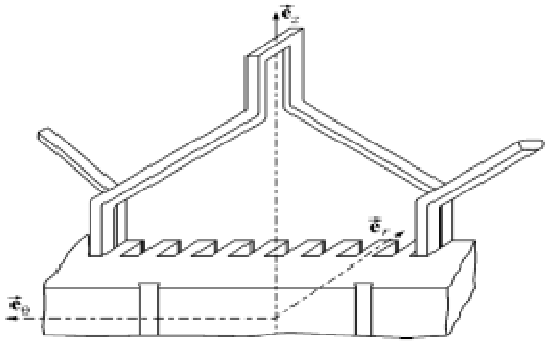

Fig. 38. Model of end-windings of turbogenerator used in simulation [40]

Two major methods used in the literatures: one presented in [17] and 2nd used the current sheets instead of the real conductors. Biot-Savart law was used in the former method, in which the iron effect in the model was taken into account by the image method. However, as mentioned in [18], considering the effect of the magnetic rotor retaining ring and rotor shaft is so complicated by image method. On the other hand, by utilizing the current sheet and using the solution of partial differential equations, it is possible to take into account the effect of iron easier than that of the image method. Since the method in [17] can be used for end-winding with any shape, it is worthwhile to develop a method for considering the iron effect instead of the image method.

Numerical methods for estimating the end-winding force are divided into four different categories; Reluctance network, integral equation method, Finite difference and FE method. First three methods are rarely used, but FEM is more accurate and applicable method. The commercial softwares based on the FEM makes can estimate the force easily and precisely.

In literatures, two ways were used to model end-region of turbogenerators, two dimensional or quasi three dimensional and three dimensional. Quasi 3D method is based on the assumption that end-region geometry of generator is axisymmetric and all electrical and magnetic parameters components have sinusoidal distribution in peripheral direction. In this method, end winding currents are replaced by the equivalent current sheets and scalar magnetic field formulation is used to solve the problem.

In 3D method, modeling real geometry of end-region is possible. It is noted that it is not necessary to model all parts of the stator core, but a fraction of the core can be modeled. Magnetic scalar potential and magnetic vector potential formulations are employed to solve the problem. In the first method, windings are represented by the filaments crossing the center of coils, and in the latter case cross section of coils is considered. Representation of coils by filaments is

easier and the calculated force is higher than representing coils by real cross section, thus estimated force is more reliable.

A fast computation is possible using 2D FE method. 2D FEM have been widely used to compute the magnetic field and force in the end-region. Normally the results of 2D FEM have good agreement with the experimental results. It is important to note that the windings currents and thus magnetic field has no sinusoidal distribution in the peripheral direction in some cases such as two-phase to ground short circuit fault which imply higher current and force level in the windings than the three-phase short circuit fault. Another restriction of 2D FEM is that the parts with no full symmetry in peripheral direction (such as teeth and slots), must be neglected or considered with some modifications.

3D method modeling of end-region of generator is very time consuming, so some simplifications almost are required. It is hope that in the future 3D calculation of the end-region magnetic field of the generator takes shorter computation time.

It may be shown that the following parameters affect the force estimation on the end-windings:

1. stator end-plate
2. rotor retaining ring
3. stator frame
4. rotor shaft
5. stepped core end
6. air gap
7. stator flux screen
8. coil cross section area
9. rotor and stator slots
10. rotor and stator core saturation
11. rotor windings (field winding, damper windings)
12. eddy current induced in solid parts
13. rotor angle
14. core depth in the model

These parameters have no identical impact on the force and some are more important than others. There is no any literature that considers all these parameters; core saturation, rotor field winding, retaining ring, rotor shaft, air gap and stator slots impact are considered more than other parameters. Stator frame and rotor angle impact are rarely considered. Sensitive analysis of the amount of each parameter impact on the magnetic force is rarely discussed.

5. SUGGESTIONS FOR FUTURE STUDIES

Considering sensitive of the developed method with taking into account effect of end-region parameters of synchronous generator such as flux-screen, end-plate is the subject of future studies, especially by 3D FEM. Compression between analytical and numerical method results and discussion about their accuracy should be carried out in more detail. In 3D FEM, effect of real number if rotor field winding in each slot, effect of stepped end-core, effect of depth of stator core in model and stator frame should be studied.

Analytical calculation of magnetic field and force on the stator end-winding using the method in [17, 18] in which iron effect in the end region is taken into account (instead of image method) can be valuable. Although the effect of induced eddy current in the rotor retaining ring has been dealt with, however, comprehensive study of it in order to obtain more precise results is significant.

REFERENCES

[1] G. Klempner, and I. Kerszenbaum, "Operation and Maintenance of Large Turbo-Generators," John Wiley & Sons Inc., 2004.

[2] M.T. Holmberg, "Three Dimensional Finite Element Computation of Eddy Currents in Synchronous Machines," Technical report, No. 350, Chalmers University of Technology.

[3] J. F. Calvert, "Forces in Turbine Generator Stator Windings," AIEE Trans., Vol. 50, pp.178-196, March 1931.

[4] D. Harrington, "Forces in Machine End Windings," AIEE Trans.,Vol. 71, part III, pp. 849-859, October 1952.

[5] P. Hammond, "Electric and Magnetic Images," Proc. Inst. Elec. Eng., Vol. 107c, Monograph No. 379, pp. 306-313, May 1960.

[6] C. J. Carpenter, "The Application of the Method of Images to Machine End-Winding Fields," Proc. Inst. Elec. Eng., Vol. 107, No. 3327, pp. 487-500, October 1960.

[7] J.B. Young, and D.H. Tompsett, "Short Circuit Forces on Turbo-generator End-Windings," Proc. Inst. Elec. Eng., Vol. 102, Part A, No. 2, pp. 101-119, April 1955.

[8] R.T. Smith, "End Component of Armature Leakage Reactance of Round-Rotor Generators," AIEE Transactions, Part III (power apparatus and systems), Vol. 77, pp.636-647, August 1958.

[9] P. Hammond, "The Calculation of Magnetic Field of Rotating Machines, Part 1: The Field of a Tabular Current," Proc. Inst. Elec. Eng., Vol. 106c, Monograph No. 333, pp. 158-164, May 1959.

[10] D. S. Ashworth and P. Hammond, "The Calculation of the Magnetic Field of Rotating Machines, part 2.—The Field of Turbo-Generator End-Windings," Proc. Inst. Elec. Eng., Vol. 108A, No. 3489, pp. 527-538, March 1961.

[11] J. A. Tegopoulos, "Determination or the Magnetic Field in the End Zone of Turbine Generators," IEEE Trans. on power apparatus and systems, Vol. 81, pp. 562-572, August 1963.

[12] J. A. Tegopoulos, "Current Sheets Equivalent to End-Winding Currents of Turbine-Generator Stator and Rotor," AIEE Trans., Vol. 81, pp. 695-700, February 1963.

[13] J. A. Tegopoulos, "Flux Impinging on the End Plate of Turbine Generators," AIEE Trans., Vol. 81, pp. 700-706, February 1963.

[14] J. A. Tegopoulos, "Magnetic Vector Potential as a Result of Elementary Currents Between Two Parallel Planes," IEEE Trans. on power apparatus and systems, Vol. 81, pp. 559-562, August 1963.

[15] J. A. Tegopoulos, "Forces on the End Winding of Turbine-Generators, I-Determination of Flux Densities," IEEE Trans. on power apparatus and systems, Vol. PAS-85, No. 2, pp. 105-113, February 1966.

[16] J. A. Tegopoulos, "Forces on the End Winding of Turbine-Generators, II-Determination of Forces," IEEE Trans. on power apparatus and systems, Vol. PAS-85, No. 2, pp. 114-122, February 1966.
[17] P. J. Lawrenson, "The Magnetic Field of the End-Windings of Turbo-Generators," Proc. Inst. Elec. Eng., Vol. 108A, No. 3490, pp. 538-549, March 1961.
[18] P.J. Lawrenson, "Forces on Turbogenerator End Windings," Proc. Inst. Elec. Eng., Vol. 112, No. 6, pp. 1144-1158, June 1965.
[19] P. B. Brandl, "Forces on the End Winding of AC Machines", Brown Boveri Review, Vol. 2, pp. 128-134, 1982.
[20] E. Nitsche, "Fields and Forces in End-windings of Synchronous Machines at sudden short-circuits," Proceedings of International Conference on electrical Machines, pp. G3/5-1- G3/5-10, 1978.
[21] H. C. Karmaker, "End Winding Fields and Forces in Salient-pole Synchronous Machines," Proceedings of International Conference on electrical Machines, Espoo, Finland, pp. 1139-1142, August 2000.
[22] A. Merkhouf, B. F. Boueri, and H. Karmaker, "Generator End Winding and Natural Frequency Analysis," Proceedings of International Conference on Electric Machines and Drives, Madison, Wisconsin, USA , pp.111-114, June 2003.
[23] X. Wen, R. Yao, and J. A. Tegopoulos, "Transient Quasi-3D Method in the Transient Electromagnetic Field Calculation of End Region of Turbo-generator," IEEE Trans. on Magnetics, Vol. 30, No. 5, pp. 3709-3712, Sept. 1994.
[24] X. Wen, R. Yao, and J. A. Tegopoulos, "Calculation of Forces on the Stator End Winding of Turbogenerator by the Transient Quasi-3D Method," IEEE Trans. on Magnetics, Vol. 32, pp. 1669-1672, May 1996.
[25] M. Freese, and A. Gruning, "Influence of the Rotor Retaining Ring on the Electromagnetic Forces in the End Winding of a Turbogenerator," 21th Symposium on Electromagnetic Phenomena in nonlinear circuits, Dortmund and Essen, Germany, 2010.
[26] K. Senske, S. Kulig, J. Hauhoff, and D. Wunsch, "Vibrational Behavior of the Turbogenerator Stator End Winding in Case of Electrical Failures," Conf. Proc. CIGRE, Yokohama, Japan, 29 October 1997.
[27] O. Drubel, S. Kulig, and K. Senske, "End Winding Deformations in Different Turbo generators during 3-phase short circuit and full load operation," Electrical Engineering, Vol. 82, pp. 145-152, Springer-Verlag 2000.
[28] A. Gruning, and S. Kulig, "Electromagnetic Forces and Mechanical Oscillations of the Stator End Winding of Turbo Generators," Springer-Verlag, pp. 115-126, 2006.
[29] K. R. Davey, "A Three Dimensional Scalar Potential Field Solution and its Application to the Turbine Generator End Region," IEEE Transactions on Power Apparatus and Systems, Vol. PAS-100, No. 5, pp. 2302-2310, May 1981.
[30] D. J. Scott, S. J. Salon, and G. L. Kusik, "Electromagnetic Forces on the Armature End Windings of Large Turbine Generators, I. steady states conditions," IEEE Trans. PAS, Vol. PAS-100, No. 1, pp.4597-4603, Nov. 1981.
[31] S. J. Salon, D. J. Scott, and G. L. Kusik, "Electromagnetic Forces on the End Windings of Large Turbine Generators, II. Transient Conditions," IEEE Transactions on Power Apparatus and Systems, Vol. PAS-102, No. 1, pp. 14-19, January 1983.
[32] G.K.M. Khan, G.W. Buckley, and N. Brooks, "Calculation of Forces and Stresses on Generator End-Windings - Part I: Force," IEEE Trans. on Energy Conversion, Vol. 4, No. 4, pp. 661-670, December 1989.
[33] S. K. Chow, Y. T. Lee, and E. A. Owen, "An Integral-Equation/Singularity-Method Approach for 3-D Electromagnetic Field determination in the End Region of a Turbine-Generator," IEEE Transactions on Magnetics, Vol. MAG-18, No. 2, pp. 340-345, March 1982.
[34] B. Frei-Spreiter, and K. Reichert, "Calculation of End Winding Field of Turbogenerators by Integral Methods for Modeling Mechanical Characteristics," IEEE Trans. on Magnetics, Vol. 34, No. 5, pp. 3636-3639, September 1998.
[35] N. Richard, F. Dufeau, A. C. Leger and N. Szylowicz, "Computation of Forces and Stresses on Generator End Windings Using a 3D Finite Element Method," IEEE Trans. on Magnetics, Vol. 32, No. 3, pp. 1689-1692, May 1996.
[36] N. Richard, "Calculation of electromagnetic forces on large generator end-windings under fault conditions using a three-dimensional finite element method," Elsevier, Mathematics and Computers in Simulation, 46, pp. 257-263, 1998.
[37] S. Richard, J.P. Ducreux, and A. Foggia, "A Three Dimensional Finite Element Analysis of the Magnetic Field in the End Region of a Synchronous Generator," Proceedings of International Conference on Electric Machines and Drives, Milwaukee, Wisconsin, USA, pp. wc2-4.1-wc2-4.3, May 1997.
[38] A. Stermecki, O. Biro, H. Lang, G. Ofner, K. Preis, and S Rainer, "Analysis of Synchronous Generator End-Winding Deformations Using 3-D Time-Harmonic FEM, " Proceedings of International Conference on Electrical Machines, Rome, Italy, Sep. 2010.
[39] Yujing Liu, and S. Hjärne, "Analysis of Forces on Coil Ends of Formed Stator Windings," Proceeding of International Conference on Electrical Machines and Systems, Seoul, South Korea, pp. 1019-1024, October 2007.
[40] R. D. Stancheva, and I. I. Iatcheva, "3-D Electromagnetic Force Distribution in the End Region of Turbogenerator", IEEE Transactions on Magnetics, Vol. 45, No. 3, pp. 1000-1003, March 2009.
[41] Z. Chong, H. Song, and Y. Yongming, "Analysis of electromagnetic forces on involute part of end winding in a 1550 MW nuclear generator", Proceedings of 2nd Advanced Information Technology, Electronic and Automation Control Conference, Chongqing, China, October, 2017.